

Clinical evaluation of the effect of attenuation correction technique on ^{18}F -fluoride PET images

Yoshibumi TAYAMA,* Nobukazu TAKAHASHI,* Takashi OKA,* Akira TAKAHASHI,**
Masato ARATAKE,** Tomoyuki SAITOU** and Tomio INOUE*

Departments of *Radiology and **Orthopaedic Surgery, Yokohama City University School of Medicine

Objective: The purpose of this study is to evaluate effect of attenuation correction technique on ^{18}F -fluoride positron emission tomography (PET). **Methods:** We performed PET scans after the injection of 185 MBq ^{18}F -fluoride on 32 patients from October 20th, 2004 to April 13th, 2005. We calculated bone-to-muscle ratios for the images with and without attenuation correction. We placed regions of interest (ROIs) on normal bone accumulation in 22 patients. The exclusion criteria were bone metastasis, Paget's disease, and rheumatoid arthritis. Several regions were chosen for ROI placement: skull, cervical vertebra, mandible, scapula, thoracic vertebra, rib, humerus, lumbar vertebra, radius, ulna, pelvis, femoral head, femoral shaft, tibia, and fibula. The count ratios of normal bones to gluteus muscle were calculated as bone-to-muscle ratios. The count ratios of abnormal skeletal lesions to gluteus muscles were calculated as bone-to-muscle ratios, while the count ratios of abnormal skeletal lesions to normal bones were calculated as bone-to-bone ratios. **Results:** PET images without attenuation correction showed significantly higher mean bone-to-muscle ratios than those with attenuation correction ($p < 0.05$) for all normal bones except the femoral head and lumbar vertebrae. For abnormal bones, bone-to-muscle ratios without attenuation correction were significantly higher than those with attenuation correction ($p < 0.005$). The same statistical significance was found for bone-to-bone ratios ($p < 0.005$). **Conclusions:** The attenuation correction technique is not necessary to conduct the visual interpretation of ^{18}F -fluoride PET images. The bone-to-muscle ratio analysis without attenuation correction may be of use to differentiate malignant from benign disease processes.

Key words: ^{18}F -fluoride, PET, attenuation correction, bone-to-muscle ratio

INTRODUCTION

Fluorine-18-fluoride ion (^{18}F -fluoride) is a bone scanning agent. Bone scanning with ^{18}F -fluoride was first introduced by Blau et al.¹ Following the development of $^{99\text{m}}\text{Tc}$ -labeled bisphosphonates in the 1970s as a superior bone-seeking radiopharmaceutical for scintigraphy, ^{18}F -fluoride was rarely used until the development of positron

emission tomography (PET) scanning. ^{18}F -fluoride PET is used to detect malignant bone disease and assess benign bone disease.

The attenuation correction technique is normally used in PET studies to improve both quantitation and uniformity in the field of view. Disadvantages of attenuation correction include errors arising from positional mismatches caused by patient motion or respiration differences, while its effect on lesion detection remains unclear. Because of low background uptake, there are few advantages of attenuation correction for bone scanning.

Tocharoenchai et al. used a hybrid PET system and found that for a phantom with hot lesions embedded in a uniform background, images using attenuation correction have decreased small lesion detectability compared to images without attenuation correction.² The aim of the

Received May 31, 2006, revision accepted November 11, 2006.

For reprint contact: Yoshibumi Tayama, M.D., Department of Radiology, Yokohama City University School of Medicine, 3-9, Fukuura, Kanazawa-ku, Yokohama, Kanagawa 236-0004, JAPAN.

E-mail: mush@k2.dion.ne.jp

present study is to evaluate the clinical detectability of ^{18}F -fluoride PET images without attenuation correction.

MATERIALS AND METHODS

Patients

Thirty-two consecutive patients (21 female, 11 male) who underwent ^{18}F -fluoride PET scans from October 20th, 2004 to April 13th, 2005 were enrolled in this study. The patients ranged in age from 20–86 years, with a mean age of 54 years.

We prospectively investigated 17 patients suspected to have tumors, five patients with bone necrosis, two patients with bone fractures, one patient with Paget's disease, two patients with osteoarthritis, and five patients with rheumatoid arthritis.

Of the patients with a suspected tumor, four had sarcoma, two had giant cell tumor, four had metastases, one had suspected hemangioma, while six had no tumor. The tumors were diagnosed surgically (six patients), by biopsy (three patients), and by observation of the clinical course (eight patients).

Radiopharmaceutical

^{18}F -fluoride for injection was produced by irradiating ^{18}O -water with protons in a metal target. After bombardment, the target water was passed through an anion-exchange resin (AG1-X8) to trap the ^{18}F -fluoride, while the isotopically enriched water was eluted and retained for reuse. ^{18}F -fluoride was eluted from the resin column with 40–200 μl of 0.5 mol/l sodium bicarbonate solution. The eluate was diluted with 10 ml of sterile isotonic saline and filtered through a 0.2- μm sterilizing filter into a sterile, pyrogen-free vial and checked for pH (pH = 6–8) and particulates. Pyrogenicity was assayed using a Limulus amoebocyte lysis assay (Associates of Cape Cod Inc., Mass., USA), and sterility was ensured by the USP sterility test method. The radiochemical and chemical purity and specific activity of the product were assayed using an AN300 high-performance liquid chromatography column (Varian, CA, USA) with 0.05 mol/l NaOH mobile phase at room temperature with suppressed conductivity and radioactivity detection.

PET scanning

PET images were obtained using a SET 2400W machine (Shimadzu, Kyoto, Japan) equipped with 20.0-cm and 59.5-cm transverse fields of view, which produced 63 image planes with a 3.125 mm interval between images. Transverse resolution at the center of the field of view was 4.2 mm, and the full width-half maximum was 5.0 mm.

A whole-body image was obtained 40 minutes after the injection of 185 MBq ^{18}F -fluoride in 10 ml of 0.9% saline solution using the multiple-bed position technique. The head to the thigh was imaged in four to five sections.

Attenuation-corrected transverse images were recon-

structed with the ordered-subsets expectation maximization algorithm into 128×128 matrices with pixel dimensions of 4.0 mm in-plane and 3.125 mm axially. Coronal images with a 9.8 mm section thickness were also reconstructed from attenuation-corrected transverse images for visual interpretation.

Data analysis

Statistical analysis. We studied images with and without attenuation correction. Elliptical regions of interest (ROIs), ranging in size from 50 to 100 pixels, were manually placed over bones and muscles to include the area with maximum counts. These maximum counts were then used for semi-quantitative analysis. We used the paired t-test to determine the statistical significance of the results. P values less than 0.05 were considered significant. The unpaired t-test was only used to determine the significant difference between standardized uptake values (SUVs) for bones of the extremities and those for bones in the trunk.

Normal bones. We placed ROIs on normal bone accumulation in 22 patients. The exclusion criteria were bone metastasis, Paget's disease, and rheumatoid arthritis, because they had or were suspected to have multiple bone disorders. We situated the ROIs in the skull, cervical vertebra, mandible, scapula, thoracic vertebra, rib, humerus, lumbar vertebra, radius, ulna, pelvis, femoral head, femoral shaft, tibia, and fibula. We placed one ROI over each lesion for the forearm and lower leg, as the radius and ulna, and tibia and fibula, could not be distinguished individually on the PET images. Mean counts of the bones on both sides of the body were used as the bone counts. In the case of a patient with a skeletal lesion on one side, counts from the contralateral normal bone were used.

The count ratios of skeletal regions to gluteus muscles were calculated as bone-to-muscle ratios. Mean counts of bilateral gluteus were used as muscle counts. Functional images of the SUV were produced using attenuation-corrected transverse images, injected doses of ^{18}F -fluoride, body weight, and cross-calibration factors between the PET scanner and the dose calibrator. SUV was defined as follows: $\text{SUV} = \text{conc}/\text{dose}/\text{wt}$, where conc is the radioactive concentration in tissue or a lesion measured in MBq per gram; dose is the injected dose measured in MBq; and wt is the patient's body weight measured in grams.

Abnormal bones. The count ratios of abnormal skeletal lesions to gluteus muscles were calculated as bone-to-muscle ratios, while the count ratios of abnormal skeletal lesions to normal bones were calculated as bone-to-bone ratios.

Comparison of interpretation. Images with attenuation correction and images without attenuation correction were interpreted by 3 physicians. These 3 observers had been reading PET for 4 years.

First, each observer reviewed images without attenuation correction. Second, after 4 weeks, they reviewed images with attenuation correction. The findings for each image were given a particular score depending on the

Table 1 Mean SUVs and bone-to-muscle ratios of ^{18}F -fluoride in normal skeletal system

Site of bone	SUV	B/M (AC-)	B/M (AC+)
Skull	2.8 ± 1.0	8.4 ± 3.3**	2.3 ± 0.9
Cervical vertebra	5.3 ± 0.8	14.8 ± 5.4**	4.5 ± 1.1
Mandible	3.1 ± 0.7	11.5 ± 4.2**	2.6 ± 0.8
Scapula	2.7 ± 0.6	3.7 ± 2.2*	2.3 ± 0.8
Thoracic vertebra	5.7 ± 1.5	6.4 ± 3.2**	4.9 ± 1.5
Rib	2.0 ± 0.5	3.3 ± 1.6**	1.6 ± 0.4
Humerus	1.5 ± 0.3	2.2 ± 1.3**	1.3 ± 0.5
Lumbar vertebra	6.0 ± 1.5	6.2 ± 3.3	5.1 ± 1.5
Radius + ulna	1.0 ± 0.2	2.4 ± 1.1**	0.9 ± 0.3
Pelvis	4.5 ± 1.2	7.0 ± 4.9**	3.8 ± 1.3
Femoral head	2.9 ± 0.9	2.2 ± 1.3	2.5 ± 1.0***
Femoral shaft	1.9 ± 0.5	2.9 ± 1.0**	1.6 ± 0.5
Tibia + fibula	1.3 ± 1.2	5.0 ± 2.3**	1.2 ± 0.4
Average	3.1 ± 1.9	5.9 ± 4.8**	2.7 ± 1.7

SUV = Standardized uptake value

B/M = Ratio of PET values in skeletal lesions to reference PET values in gluteus muscles

AC- = Without attenuation correction

AC+ = With attenuation correction

* = Significantly higher than ratios with attenuation correction using paired t-test ($p < 0.05$)

** = Significantly higher than ratios with attenuation correction using paired t-test ($p < 0.01$)

*** = Significantly higher than ratios without attenuation correction using paired t-test ($p < 0.05$)

likelihood of abnormality (1, definitely normal; 2, probably normal; 3, equivocal; 4, probably abnormal; 5, definitely abnormal).

One region of each image was designated to review. Even if the other region seemed definitely abnormal and the designated region seemed normal, observers did not review non-designated regions. These designated regions were 10 regions with tumor, 6 regions with necrosis, 5 regions with fracture, 4 regions with rheumatoid arthritis, 2 regions with spondylosis, 1 region with osteoarthritis, 1 region with Paget's disease, 1 region with suspected hemangioma on MR and 3 regions without disease.

We defined the regions with score 4 and 5 as abnormal findings. Sensitivity and specificity were calculated from the interpretations.

RESULTS

The SUV of normal bones was 3.1 ± 1.9 (mean \pm SD). The mean SUVs for cervical, thoracic, and lumbar vertebrae were greater than 5.0 (Table 1). The pelvis recorded the next highest SUV: 4.5 ± 1.2 . The SUVs for the mandible, femoral head, skull, and scapula were moderate: 2.7 to 3.1. The SUVs in the bones of the extremities (1.5 ± 0.5) were significantly lower than those in the bones of the trunk (3.9 ± 1.8 ; $p < 0.0001$).

In all normal bones except for the femoral heads and lumbar vertebrae, mean bone-to-muscle ratios without attenuation correction were significantly higher than those with attenuation correction ($p < 0.05$; Table 1). Bone-to-muscle ratios without attenuation correction in the skull, cervical vertebra, mandible, rib, radius, ulna, femur,

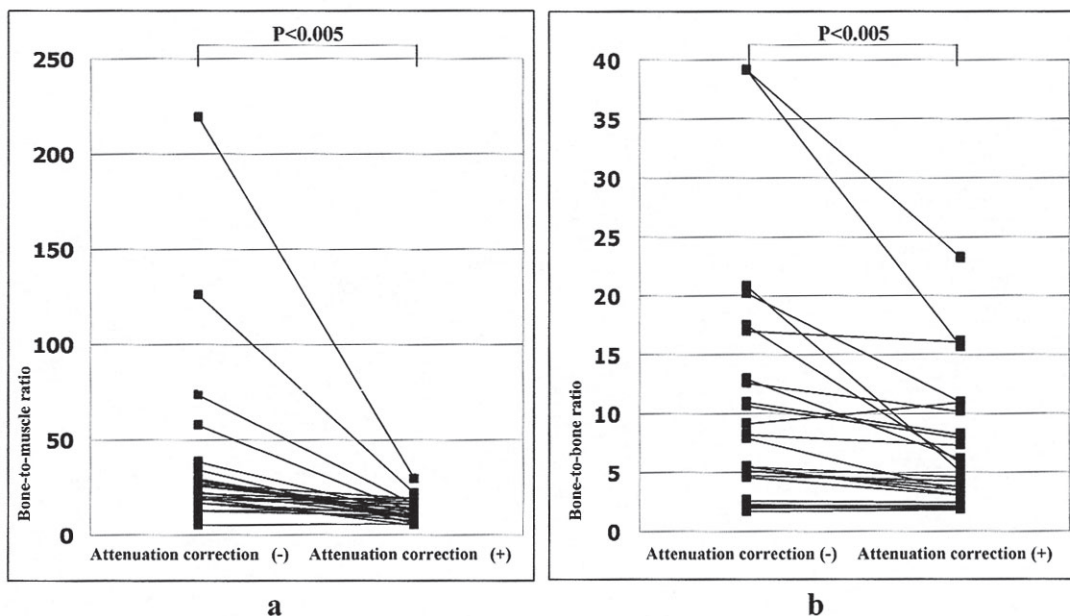
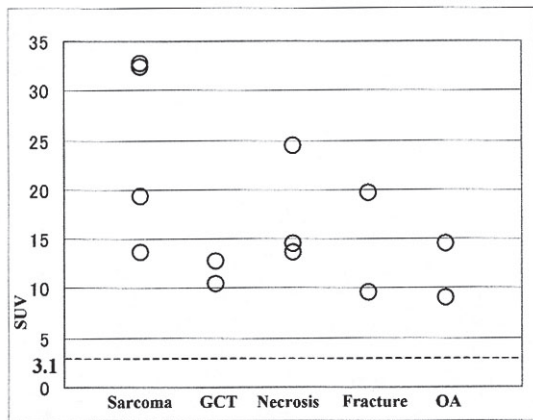
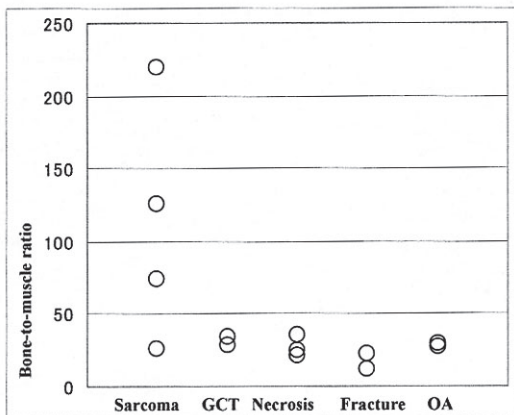


Fig. 1 Count ratios of skeletal lesions to gluteus muscles (a) and count ratios of skeletal lesions to normal bones (b) without and with attenuation correction.

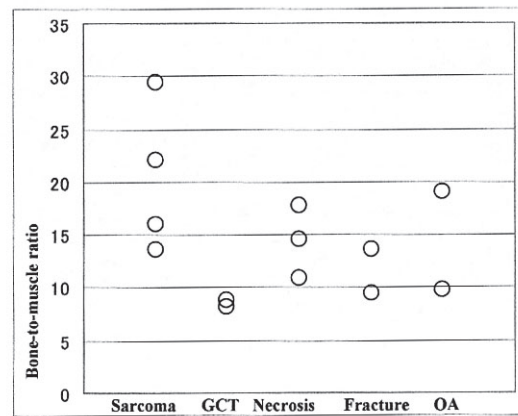


The SUV of normal bones was 3.1 ± 1.9 (mean \pm SD).

a



b



c

Fig. 2 SUVs (a), bone-to-muscle ratios without attenuation correction (b), and bone-to-muscle ratios with attenuation correction (c), for sarcoma, giant cell tumor, necrosis, fracture, and osteoarthritis.

and tibia and fibula were much higher than those with attenuation correction ($p < 0.0001$).

In abnormal bones, bone-to-muscle ratios without attenuation correction were significantly higher than those with attenuation correction ($p < 0.005$; Fig. 1a). The result was the same in abnormal-to-normal bone ratios ($p < 0.005$; Fig. 1b).

Sarcomas demonstrated the highest uptake (24.5 ± 9.62 ; Fig. 2a), followed by necroses (18.0 ± 6.0 ; Fig. 2a).

For all diseases, the mean bone-to-muscle ratio without attenuation correction was higher than that with attenuation correction (Figs. 2b, 2c).

Regarding comparison of image interpretation, in 9 of 33 cases, at least one observer assigned different scores to images with attenuation correction and images without attenuation correction.

One observer assigned different scores (3 points higher) on images without attenuation correction in a case. In other 8 cases, observers assigned 1 point higher or lower on images without attenuation correction. In 6 cases, at least one observer assigned a higher score on images without attenuation correction than images with attenuation correction. Five of those 6 cases had osteochondritis

dissecans, coxarthrosis, neurogenic tumor, rheumatoid arthritis, spondylosis. The other one showed abnormal MR signal intensity, and we suspected hemangioma.

In 4 cases, one observer assigned a higher score on images with attenuation correction than images without attenuation correction, and 2 cases showed false positive results. Other 2 cases had a femoral neck fracture and cervical spondylosis.

Sensitivity of images without attenuation correction was 85.6%, and that of images with attenuation correction was 83.3%. In 10 cases, designated regions were bones with a malignant or benign tumor. High sensitivities were showed in those cases by images without attenuation correction (93.3%) and with attenuation correction (90.0%). Sensitivities for spondylosis were low for images without attenuation correction (16.7%) and with attenuation correction (0%).

Specificities of images with attenuation correction and those without attenuation correction were 88.9%.

DISCUSSION

The skeletal system is in a permanent state of dynamic

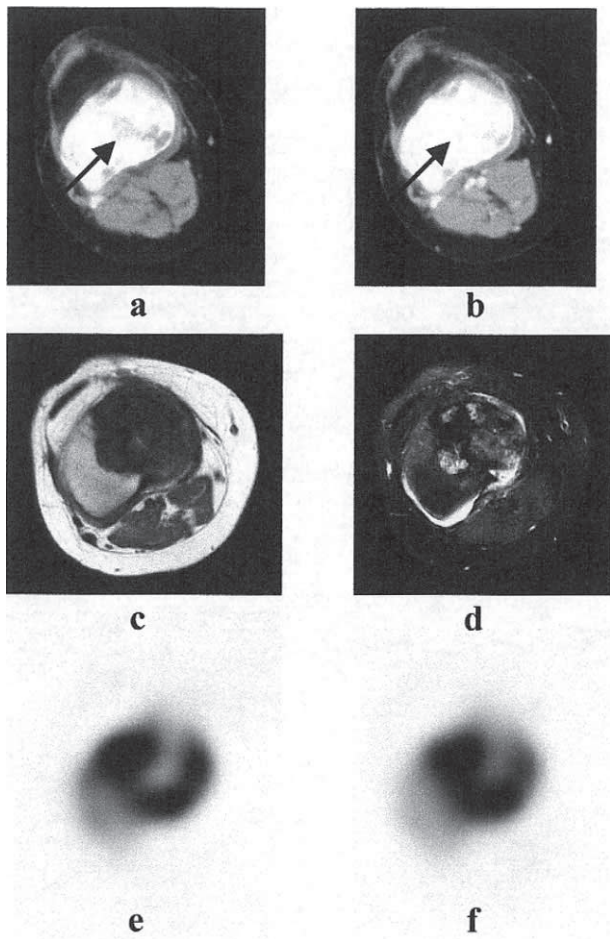


Fig. 3 Images of an osteosarcoma in the right tibia of a 34-year-old woman with osteosarcoma in the right tibia. A plain CT image (a) reveals an osteoclastic lesion situated in the right medial tibial condyle (*arrow*). Enhancement is shown on the contrast CT image (b). A T1-weighted MR image (c) reveals the low-intensity tumor situated in the medial tibial condyle. A T2-weighted MR image (d) shows mixed intensities. A PET image with attenuation correction (e) demonstrates high peritumoral uptake. A PET image without attenuation correction (f) shows stronger contrast between the peritumoral area and other areas compared to the PET image with attenuation correction.

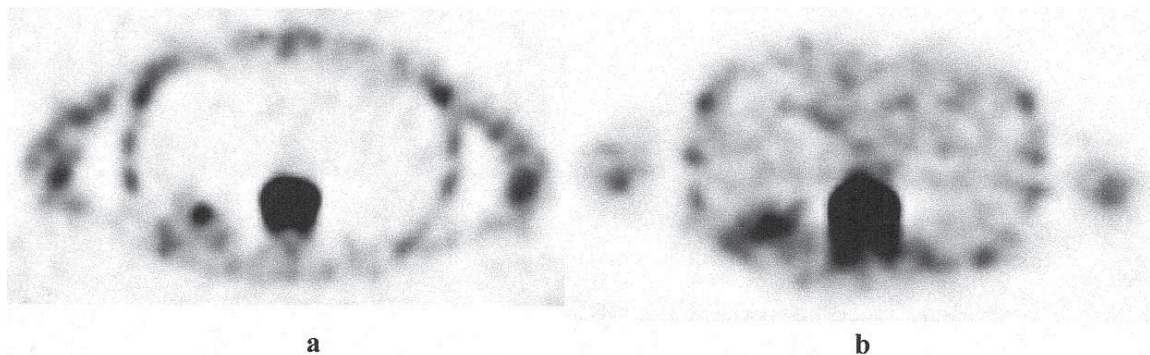


Fig. 4 Images of a 60-year-old man with T11 vertebral compression fracture. A PET image with attenuation correction (a) demonstrates abnormally increased accumulations in the thoracic vertebrae. A PET image without attenuation correction (b) shows similar findings.

equilibrium between bone formation and resorption. ^{18}F -fluoride is extracted from plasma in proportion to bone perfusion,³⁻⁶ and is used as a measure of bone metabolism. In reflecting the physiologic process, the compartment model describes fluoride kinetics from the plasma into the unbound bone compartment followed by ionic exchange of the fluoride with the hydroxyl group in hydroxyapatite to form fluoroapatite.^{7,8} ^{18}F -fluoride is clinically useful because of its high sensitivity and specific modality for detection of bone metastases from lung, breast, renal, bladder, and prostate cancer.⁹⁻¹⁵ ^{18}F -fluoride PET is also highly cost-effective for the detection of bone metastases in lung cancer.¹⁴ In cases of prostatic cancer, when PSA is greater than 20 ng/ml in patients with a high suspicion of osseous metastases, ^{18}F -fluoride PET provides a sensitive and cost-effective method of evaluation.¹² Wootton et al. demonstrated that plasma clearance estimates of ^{18}F -fluoride kinetics are useful in monitoring the response of Paget's disease to calcitonin therapy,¹⁶ while ^{18}F -fluoride uptake has been found to correlate with the work rate of osteoblasts in idiopathic or postmenopausal osteoporosis.¹⁷ ^{18}F -fluoride PET shows the direct metabolic effect of antiresorptive therapy on skeletal kinetics at the clinically important site of the lumbar spine.¹⁸

In the present study, sarcomas revealed higher uptakes than giant cell tumors. These high accumulations did not reflect uptake in the sarcoma itself, but reflected remodeling of bone destroyed by sarcoma invasion. Brener also reported high FDG and ^{18}F -fluoride uptake in sarcomas,¹⁹ as observed in our results.

We observed much higher bone-to-muscle ratios in images without attenuation correction than in images with attenuation correction in seven sites of normal bone; these were superficial bones. In contrast, for two normal bone sites we did not observe significantly higher bone-to-muscle ratios without attenuation correction compared to images with attenuation correction; these were profound bones. We postulate that differences in bone-to-muscle ratios between images with and without attenuation correction are related to bone depth.

The sensitivity of planar bone scintigraphy in the detection of malignant osseous lesions in the skull, thorax, and extremities is 82.8%, with a sensitivity of 40% in the spine and pelvis.²⁰ No planar bone scintigraphy employs attenuation correction; consequently, there was some attenuation effect that revealed a lower sensitivity for profound lesions. We consider that attenuation correction is not necessary to detect superficial lesions.

The ¹⁸F-fluoride PET images without attenuation correction tended to demonstrate higher contrast between the hyper-accumulated lesions and their circumference than images with attenuation correction. This occurs because of the lower count in organs other than bone. Difficulties encountered in determining the position of a lesion may be solved using the PET-CT system. The images without attenuation correction also demonstrated higher contrast between abnormal bone and contralateral bones. In conclusion, abnormal bones showed high contrast against other structures.

The bone-to-muscle ratio analysis appears useful to differentiate sarcomas from benign diseases; however, it may only reflect the position of the lesion. In this study, three of four sarcomas were in the distal lower extremities (talus, tibia and fibula). Another sarcoma was located in the pelvis, which recorded the lowest bone-to-muscle ratio without attenuation correction. Further study with a larger number of patients is required to evaluate significant differences in detection among different diseases.

Regarding comparison of image interpretation, in 6 of 33 cases, images without attenuation correction showed better results than images with attenuation correction in the detection of abnormalities. All of the 6 cases were showed abnormal findings on either one of the CT, MRI, X-ray photograph or bone scan.

One observer assigned a higher score on images without attenuation correction and images with attenuation correction in 4 of 33 cases, but 2 of the 4 cases did not show abnormal findings on the following studies. In these 2 cases, images without attenuation correction showed 'better' findings than images with attenuation correction.

The sensitivity without attenuation correction was higher than that with attenuation correction.

It seems that images without attenuation correction are clinically useful to detect abnormal lesions.

CONCLUSIONS

The attenuation correction technique is not necessary for visual interpretation of ¹⁸F-fluoride PET images. The bone-to-muscle ratio analysis without attenuation correction may be of use to differentiate malignant from benign disease processes.

REFERENCES

1. Blau M, Nagler W, Bender MA. Fluorine-18: a new isotope

- for bone scanning. *J Nucl Med* 1962; 3: 332–334.
2. Tocharoenchai C, Tsui BM, Frey EC, Wang WT. Effect of attenuation correction on lesion detection using a hybrid PET system. *J Med Assoc Thai* 2005; 88: 96–102.
3. Green JR, Reeve J, Tellez M, Veall N, Wootton R. Skeletal blood flow in metabolic disorders of the skeleton. *Bone* 1987; 8: 293–297.
4. Nahmias C, Cockshott WP, Belbeck LW, Garnett ES. Measurement of absolute bone blood flow by positron emission tomography. *Skeletal Radiol* 1986; 15: 198–200.
5. Wootton R, Dore C. The single-passage extraction of ¹⁸F in rabbit bone. *Clin Phys Physiol Meas* 1986; 7: 333–343.
6. Wootton R, Reeve J, Veall N. The clinical measurement of skeletal blood flow. *Clin Sci Mol Med* 1976; 50: 261–268.
7. Hawkins RA, Choi Y, Huang SC, Hoh CK, Dahlbom M, Schiepers C, et al. Evaluation of the skeletal kinetics of fluorine-18-fluoride ion with PET. *J Nucl Med* 1992; 33: 633–642.
8. Cook GJ, Lodge MA, Blake GM, Marsden PK, Fogelman I. Differences in skeletal kinetics between vertebral and humeral bone measured by ¹⁸F-fluoride positron emission tomography in postmenopausal women. *J Bone Miner Res* 2000; 15: 763–769.
9. Schirrmeister H, Glatting G, Hetzel J, Nussle K, Arslanemir C, Buck AK, et al. Prospective evaluation of the clinical value of planar bone scans, SPECT, and ¹⁸F-labeled NaF PET in newly diagnosed lung cancer. *J Nucl Med* 2001; 42: 1800–1804.
10. Schirrmeister H, Guhlmann A, Kotzerke J, Santjohanser C, Kuhn T, Kreienberg R, et al. Early detection and accurate description of extent of metastatic bone disease in breast cancer with fluoride ion and positron emission tomography. *J Clin Oncol* 1999; 17: 2381–2389.
11. Even-Sapir E, Metser U, Mishani E, Lievshitz G, Lerman H, Leibovitch I. The detection of bone metastases in patients with high-risk prostate cancer: ^{99m}Tc-MDP planar bone scintigraphy, single- and multi-field-of-view SPECT, ¹⁸F-Fluoride PET, and ¹⁸F-Fluoride PET/CT. *J Nucl Med* 2006; 47: 287–297.
12. Schoder H, Larson SM. Related Articles. Positron emission tomography for prostate, bladder, and renal cancer. *Semin Nucl Med* 2004; 34: 274–292.
13. Seto E, Segall GM, Terris MK. Related Articles. Positron emission tomography detection of osseous metastases of renal cell carcinoma not identified on bone scan. *Urology* 2000; 55: 286.
14. Hetzel M, Arslanemir C, Konig HH, Buck AK, Nussle K, Glatting G, et al. F-18 NaF PET for detection of bone metastases in lung cancer: accuracy, cost-effectiveness, and impact on patient management. *J Bone Miner Res* 2003; 18: 2206–2214.
15. Schoder H, Larson SM. Positron emission tomography for prostate, bladder, and renal cancer. *Semin Nucl Med* 2004; 34 (4): 274–292.
16. Wootton R, Reeve J, Spellacy E, Tellez-Yudilevich M. Skeletal blood flow in Paget's disease of bone and its response to calcitonin therapy. *Clin Sci Mol Med* 1978; 54: 69–74.
17. Reeve J, Arlot M, Wootton R, Edouard C, Tellez M, Hesp R, et al. Skeletal blood flow, iliac histomorphometry, and strontium kinetics in osteoporosis: a relationship between

- blood flow and corrected apposition rate. *J Clin Endocrinol Metab* 1988; 66: 1124–1131.
18. Frost ML, Cook GJ, Blake GM, Marsden PK, Benatar NA, Fogelman I. A prospective study of risedronate on regional bone metabolism and blood flow at the lumbar spine measured by ^{18}F -fluoride positron emission tomography. *J Bone Miner Res* 2003; 18: 2215–2222.
 19. Brenner W, Bohuslavizki KH, Eary JF. PET imaging of osteosarcoma. *J Nucl Med* 2003; 44: 930–942.
 20. Schirmmeister H, Guhlmann A, Elsner K, Kotzerke J, Glatting G, Rentschler M, et al. Sensitivity in detecting osseous lesions depends on anatomic localization: planar bone scintigraphy versus ^{18}F PET. *J Nucl Med* 1999; 40 (10): 1623–1629.